

Plans for a 10-m Submillimeter-wave Telescope at the South Pole

Antony A. Stark^a, John E. Carlstrom^b, Frank P. Israel^c, Karl M. Menten^d,
Jeffrey B. Peterson^e, T. G. Phillips^f, Giorgio Sironi^g and Christopher K. Walker^h

^aSmithsonian Astrophysical Observatory, 60 Garden St. MS78, Cambridge, MA 02138, USA

^bUniversity of Chicago, Department of Astronomy and Astrophysics,
5640 S. Ellis Ave., Chicago, IL 60613, USA

^cSterrewacht Leiden, Postbus 9513, 2300 RA, Leiden, the Netherlands

^dMax-Planck-Institut für Radioastronomie, Auf dem Hügel 69, 53121 Bonn, Germany

^eCarnegie Mellon University, Department of Physics, Pittsburgh, PA 15213-3890, USA

^fDowns Laboratory of Physics, California Institute of Technology, Pasadena, CA 91125, USA

^g Università Degli Studi di Milano, Dipartimento di Fisica,
Sezione di Astrofisica Relativistica e Cosmologia, Via Celoria 16, 20133 Milano, Italy

^hSteward Observatory, University of Arizona, Tucson, AZ 85721, USA

ABSTRACT

A 10 meter diameter submillimeter-wave telescope has been proposed for installation and scientific use at the NSF Amundsen-Scott South Pole Station. Current evidence indicates that the South Pole is the best submillimeter-wave telescope site among all existing or proposed ground-based observatories. Proposed scientific programs place stringent requirements on the optical quality of the telescope design. In particular, reduction of the thermal background and offsets requires an off-axis, unblocked aperture, and the large field of view needed for survey observations requires shaped optics. This mix of design elements is well-suited for large-scale (square degree) mapping of line and continuum radiation from submillimeter-wave sources at moderate spatial resolutions (4 to 60 arcsecond beam size) and high sensitivity (milliJansky flux density levels). The telescope will make arcminute angular scale, high frequency Cosmic Microwave Background measurements from the best possible ground-based site, using an aperture which is larger than is currently possible on orbital or airborne platforms. The telescope design is homologous. Gravitational changes in pointing and focal length will be accommodated by active repositioning of the secondary mirror. The secondary support, consisting of a large, enclosed beam, permits mounting of either a standard set of Gregorian optics, or prime focus instrumentation packages for CMBR studies. A tertiary chopper is located at the exit pupil of the instrument. An optical design with a hyperboloidal primary mirror and a concave secondary mirror provides a flat focal surface. The relatively large classical aberrations present in such an optical arrangement can be small compared to diffraction at submillimeter wavelengths. Effective use of this telescope will require development of large (1000 element) arrays of submillimeter detectors which are background-limited when illuminated by antenna temperatures near 50 K.

Keywords: Antarctic, South Pole, submillimeter, astronomy, telescopes

1. INTRODUCTION

Of all ground-based observatory sites that have been tested for submillimeter-wave sky quality, the best results have come from the Amundsen-Scott South Pole Station. In the current decade, a year-round observatory has been established at the Pole by the Center for Astrophysical Research in Antarctica (CARA), an NSF Science and Technology Center. CARA operates three major telescope facilities: AST/RO (the Antarctic Submillimeter Telescope and Remote Observatory, a 1.7-m telescope¹), Python (a Cosmic Microwave Background experiment), and

Other author information:

A.A.S. (correspondence): E-mail: aas@cfa.harvard.edu; WWW: <http://cfa-www.harvard.edu/~aas/tenmeter/tenmeter.html>

SPIREX (the South Pole Infrared Explorer, a 60-cm telescope). These facilities are conducting site characterization and astronomical investigations from millimeter wavelengths to the near-infrared.² Profiles of temperature, pressure, and water vapor above the Pole have been measured at least daily for decades by the South Pole meteorology office.³ Measured water vapor values are extremely low because the air is desiccated by frigid temperatures (annual average: -49C, median winter PWV: 0.25mm). Winds at the Pole are unusually low (maximum recorded wind speed over 30 years: 25 m/s), and rain is completely absent.³ Atmospheric opacity at the Pole has been routinely measured at 225 GHz and 492 GHz using skydip techniques.^{2,4,5,6} The 225 GHz results are comparable to those made at the proposed NRAO Millimeter Array site at Atacama, Chile. This, together with the significantly higher atmospheric pressure at the Pole, necessarily implies that the PWV and submillimeter-wave opacity at the Pole are somewhat better than at Atacama.

A wide-field, off-axis 10 m diameter submillimeter-wave telescope has been proposed for the South Pole by an international consortium. The South Pole 10 m (SP 10m) telescope will be a powerful and highly flexible instrument, usable for a wide variety of submillimeter observations in observational cosmology, star formation, chemistry and dynamics of the interstellar medium, galactic structure, and solar system studies. The SP 10m telescope will be optically superior to existing telescopes with respect to scattered radiation, cross-polarization, and field of view and will be located at a site which is consistently much more transparent in the submillimeter-wave atmospheric windows than any other existing or proposed observatory site.² It will therefore be orders of magnitude faster than existing instruments and capable of detecting much weaker sources. It will greatly enhance submillimeter-wave capability in the Southern Hemisphere and provide a single-dish complement to the Smithsonian Astrophysical Observatory (SAO) Submillimeter Array (SMA) and the NRAO Millimeter Array (MMA). It will make use of large, sensitive bolometer and heterodyne array detectors which are advanced versions of those currently in use on the Caltech Submillimeter Observatory (CSO) and the James Clerk Maxwell Telescope (JCMT). The 10 meter telescope will be able to feed 1000 pixels in a detector array.

2. SCIENCE GOALS FOR THE SP 10M

A workshop was held at Harvard University on 28 March 1997 to discuss science goals for the SP 10m project. Some critical projects that drive the telescope design are:

Primary cosmic microwave background anisotropy at arcminute scales. At angular scales near 0.5° , standard cosmological models predict relatively large anisotropy caused by an acoustic “bounce” that occurred before recombination. The spatial frequency at which this peak occurs depends on the fundamental cosmological parameter Ω . Additional smaller peaks are expected at multiples of the peak spatial frequency. Present CMBR observations show a clear maximum in the anisotropy spectrum at a spatial scale somewhere near 1° , but the spectrum lacks detail and the harmonic peaks at smaller scales have not yet been seen. The SP 10m will study the damping tail region at arcminute scales, providing a strong test of the acoustic oscillation model and providing measurements of peak positions that will augment the lower spatial frequency information obtained with meter-class telescopes. Data from the SP 10m will be particularly vital if the universe turns out to be open, and the main spatial frequency peak occurs at scales near 0.1° . To study primary anisotropy at arcminute angular scales, it will be important to simultaneously understand the secondary contribution to anisotropy due to Sunyaev-Zel’dovich (S-Z) distortion in galaxy clusters between the recombination last scattering surface and the observer. Because of the low sky noise available at the Pole, the SP 10m can be used over a wide range of frequencies, including the 200-300 GHz range of frequencies required to allow spectral separation of thermal S-Z effect from primary anisotropy. Since there are 10^4 to 10^5 visible clusters of galaxies, both the small beam size and wide spectral range of the SP 10m will be needed to locate the cluster-free regions of sky that will be observed for primary anisotropy studies.

Sunyaev-Zel’dovich effect. As CMB photons travel from the surface of last scattering to the observer, secondary anisotropies can arise due to the interaction of the CMB photons with intervening matter. Of particular interest is the S-Z effect, which occurs when CMB photons travel through a cluster of galaxies.⁷ Approximately 10% of the total mass of rich clusters of galaxies is in the form of hot ($\sim 10^8$ K) ionized plasma. Compton scattering of CMB photons by electrons in this intra-cluster plasma can result in an optical depth as high as 0.02, resulting in a distortion of the CMB spectrum at the mK level.

There are two components of the S-Z effect which result from the two distinct velocity components of the scattering electrons. The thermal component is due to the thermal (random) velocities of the scattering electrons. The kinematic component is due to the bulk velocity of the intra-cluster gas with respect to the rest frame of the CMB. The two S-Z components have distinct spectra which can be separated by observations at millimeter wavelengths.

The thermal component of the S-Z effect can be used in combination with X-ray data to provide a measure of the Hubble constant (H_0). In addition, when combined with a measurement of electron temperature, the ratio of the kinematic and thermal component amplitudes provides a direct measurement of the cluster's peculiar velocity relative to the rest frame of the CMB. The observed surface brightness difference of both the thermal and kinematic components is independent of the cluster redshift, as long as the cluster is resolved. Using the SP 10m, accurate S-Z measurements can be made throughout the Universe, all the way back to the epoch of formation of the hot intra-cluster gas. This will be an important new probe of universal structure formation processes: a sample of peculiar velocities throughout the Hubble volume.

Continuum detection of high redshift protogalaxies not detectable in the visible or near-IR. The majority of the luminosity resulting from the collapse energy of galaxies and the first generations of stars may not appear at visual or near-infrared wavelengths (even in the rest frame of the distant galaxy), but may instead be reradiated by dust.^{8,9} Submillimeter-wave point sources with no bright visible counterpart may already have been detected.¹⁰ In the broadband rest-frame spectrum of normal galaxies are two roughly equal flux peaks: visible light produced by stars, and far-infrared radiation near $100\mu\text{m}$ produced by dust and the fine-structure cooling lines of the interstellar medium. To understand the nature of protogalaxies, it will be necessary to observe them at submillimeter, near-infrared, and visible wavelengths. The energetics of protogalaxy formation will not be understood until there is a deep, high-resolution survey of the submillimeter-wave background.^{11,12,13,14,15}

Line detection of high redshift protogalaxies not detectable in the visible or near-IR. The $^2P_{3/2} \rightarrow ^2P_{1/2}$ line of [C II] at $\lambda = 158\mu\text{m}$ is the brightest emission line in the spectrum of most galaxies. From the radio to X-ray, the wavelength of highest flux density in a galaxian spectrum is usually the peak of this line; as much as 0.5% of the total luminosity of a galaxy can be emitted in the single spectral line.^{16,17} The [C II] line-to-continuum ratio is high in low metallicity systems, so that line searches for protogalaxies may be more efficient than continuum searches.^{18,19,20} Measurement of the [C II] line yields chemical and kinematic information for galaxies detected by other means.

Continuum survey of cloud cores. An unbiased wide-area continuum survey at $\lambda = 350\mu\text{m}$ of all nearby molecular regions to identify dense cloud cores should be able to locate all such regions within 500 pc of the Sun. This project can best be carried out at a wavelength of $\simeq 350\mu\text{m}$; observing at this relatively long wavelength will ensure that even the most heavily obscured (deeply embedded) sources will be included. The SP 10m will be particularly capable of tracing extended protostellar disks, and connections between these disks and surrounding, placental material. Follow-on studies at $200\mu\text{m}$ wavelength may help discriminate among protostellar models.

A spectral line survey of detected cloud cores in kinematic tracers of the star-forming gas. Such a survey would enable discrimination among the variety of complex motions found in these regions, and in particular, identification of objects in which infall of material is occurring.

Thermal balance of star-forming regions: cooling line inventory and PDR studies. Theoretical studies have established the importance of molecular cooling in the initial phases of star formation; cooling at densities $\geq 10^6\text{cm}^{-3}$ is by a large number of lines of many different species.

Observations of the ionized nitrogen line near 1.46 THz (205 μm). The winter South Pole sky becomes 30% transparent at this frequency. The [N II] line will be a powerful probe in conjunction with observation of [C II] from SOFIA and [C I]. These observations can be used to help determine the astrophysically important carbon to oxygen ratio and are relevant for studies of the Milky Way and external galaxies.

Table 1. Continuum Sensitivity of Submillimeter Telescopes

Telescope	A^a	R^b	S^c	NEFD ^d			Time in hours to survey		
	(m ²)	($''$)		(mJy s ^{1/2})			1 square degree at 1 mJy		
				850 μ m	450 μ m	350 μ m	850 μ m	450 μ m	350 μ m
SP 10 m	79	11	38	<i>60</i>	<i>64</i>	<i>74</i>	<i>95</i>	<i>108</i>	<i>144</i>
SP 30 m	711	4	4	<i>7</i>	<i>7</i>	<i>8</i>	<i>11</i>	<i>12</i>	<i>16</i>
AST/RO	2	65	92	<i>2160</i>	<i>2300</i>	<i>2660</i>	5.1×10^4	5.8×10^4	7.7×10^4
JCMT	177	7	5	80	700	760	1.3×10^3	9.8×10^4	1.2×10^5
CSO	79	11	11	<i>150</i>	2000	<i>2200</i>	2.0×10^3	3.6×10^5	4.4×10^5
SOFIA	5	44	50		<i>200</i>	<i>200</i>		<i>800</i>	<i>800</i>
FIRST	7	32	4.3		<i>54</i>	<i>54</i>		<i>678</i>	<i>583</i>
SMA	227	2	0.14	<i>134</i>	<i>1142</i>	<i>1250</i>	3.6×10^4	9.3×10^6	1.9×10^7
MK array ^e	483	0.5	0.02	<i>59</i>	<i>719</i>	<i>790</i>	4.9×10^4	2.6×10^7	5.2×10^7
“small” MMA	2010	0.2	0.08	<i>7</i>	<i>45</i>	<i>52</i>	<i>230</i>	3.4×10^4	7.5×10^4
“large” MMA	7000	0.2	0.06	<i>2</i>	<i>12</i>	<i>15</i>	<i>19</i>	2.4×10^3	6.4×10^3

Notes:

a. Telescope area (m²)

b. Resolution element (arcsec) for $\lambda = 450\mu\text{m}$. Resolution element scales as λ .

c. Instantaneous sky coverage (arcmin²) for $\lambda = 450\mu\text{m}$. Instantaneous Sky Coverage scales as λ^2 for interferometers, is independent of λ for most single-dish instruments, and is 4.3, 5.0 and 2.7 arcmin² at 480 μm , 350 μm and 250 μm , respectively, for FIRST (G. Pilbratt, personal communication).

d. Noise Equivalent Flux Density, the sensitivity to point sources whose positions are known. Numbers in italics are predicted sensitivities; numbers not in italics are measured, on-the-telescope values and are subject to downward revision with improved techniques. Predicted sensitivities are optimistic in the sense that in all cases they are near the thermal background limit, a limit that has not yet been achieved in practical submillimeter-wave bolometer systems. This table is based on the work of Hughes and Dunlop.¹⁴

e. Mauna Kea array consisting of the SMA, the CSO and the JCMT

Polarization studies. The optical design of the 10 m telescope makes it particularly well-suited for measurement of extended polarized submillimeter-wave radiation. During the past decade, it has been demonstrated that measurement of linear polarization of the thermal emission from interstellar dust grains yields unique information concerning the configuration of magnetic fields in star-forming regions.²¹ Theoretical work suggests that these fields may determine the masses of the stars that form.²² In regions with strong, ordered fields, the theory predicts that low-mass stars will form. When the fields are weaker, they are overwhelmed by gravity and higher mass stars result. The angular resolution and sensitivity of the South Pole 10 m telescope will allow polarimetric studies to be extended from high-mass star-forming regions (where magnetic fields have been studied in detail with airborne telescopes at far-infrared wavelengths and the large submillimeter telescopes on Mauna Kea), to the fainter, more extended regions where low-mass stars are born. The comparison will provide a crucial test for theories of star formation.

High resolution submillimeter-line studies of star-forming regions in the Magellanic Clouds. The SP 10m provides an unparalleled opportunity to study star formation in a low-metallicity system—perhaps an analog of star formation in early galaxies. These observations would be made in conjunction with the MMA.

3. TELESCOPE SENSITIVITY

A 10 meter diameter telescope equipped with modern submillimeter-wave detectors and operating at the South Pole in winter is capable of detecting both line and continuum radiation from protogalaxies at $z \sim 3$ in less than an hour. A protogalaxy which will evolve into a large (L^*) galaxy produces a continuum flux density of about 5 mJy and a [C II] line power of about 1 K km s⁻¹ at the focus of a 10 meter telescope.²⁰ AST/RO has already detected submillimeter spectral lines having 0.5 K km s⁻¹ power.²³ Even though this power level corresponds to a

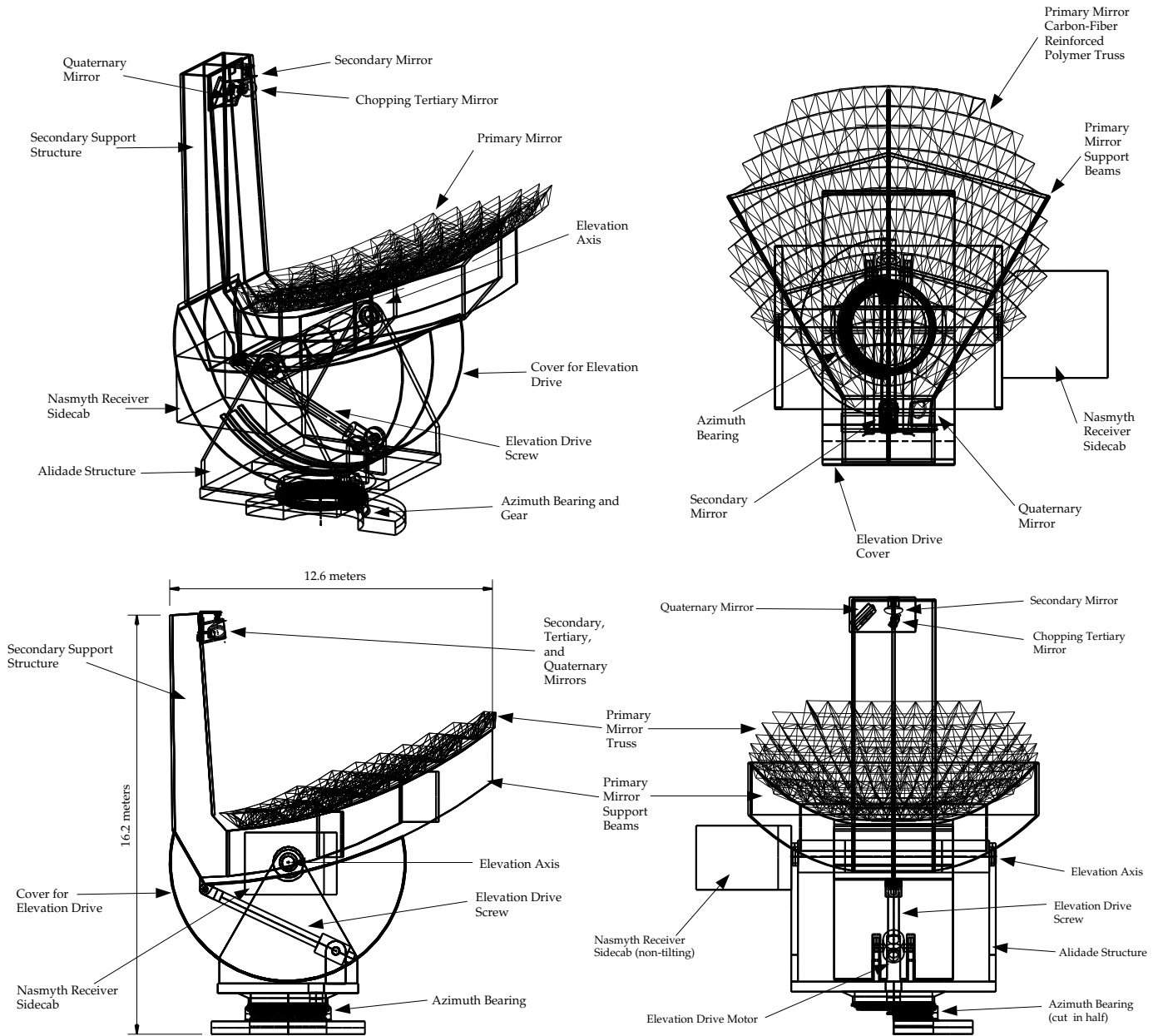


Figure 1. A Computer Model of the South Pole 10 meter Telescope.

significantly larger flux in the beam of a 1.7 meter telescope, detection of these lines with AST/RO demonstrates that an offset 10 meter antenna operating under the winter South Pole sky can overcome systematic noise problems at this power level and is capable of making observations of the requisite sensitivity for observing protogalaxies.

Table 1 shows the continuum sensitivity and beam size of the SP 10m and other submillimeter-wave telescopes and illustrates the strength of the SP 10m for deep continuum surveys. The NEFD values in this table result from different assumptions for the different instruments, assumptions which have varying degrees of certainty and practical verification; it should be understood that this table is speculative. The high sensitivity per pixel for the SP 10m results from the combination of a relatively large aperture, large available bandwidth, and fairly good sky; the fast survey speed results from high sensitivity and a large field of view; a relatively small beam size provides freedom from confusion. This combination of attributes assures that the SP 10m telescope will make unique and important contributions to astronomy.

4. DESIGN CONCEPT

A design study was conducted in 1996 by the SAO Central Engineering Department using funding contributed for that purpose by the Smithsonian Institution. That study has resulted in a preliminary design for the telescope, a static structural analysis of the design, a detailed seven year budget, and a plan for the construction of the telescope using the technology, personnel, and facilities currently being used to construct the six 6-m diameter antennas of the Submillimeter Array (SMA).

Avoidance of internal reflections is critical to the design of submillimeter-wave telescopes. Any receiver or detector placed at the focus of the instrument will necessarily emit into the telescope some amount of submillimeter-wave power in the band of interest. If there is a reflection in the system, for example at the secondary mirror some 6 meters distant, then a resonant cavity is formed whose modes are spaced at roughly 25 MHz intervals, and spurious features at those intervals will appear in the spectrometer whenever there is a change in power level or cavity dimensions. Submillimeter-wave spectrometers cover more than 1 GHz of bandwidth, and a 25 MHz spurious feature can masquerade as a typical astronomical or atmospheric line. Also critical to submillimeter-wave telescope design is minimization of variations in antenna thermal emissions as a function of chopper angle. Chopper offsets can more easily be minimized in an off-axis design.

Dragone²⁴ has shown that if the offset angles in an offset Gregorian antenna are chosen correctly, then aberrations and cross-polarization effects in that offset antenna are the same as those in a conventional on-axis antenna with the same diameter and focal length. The beam efficiency, aperture efficiency, and sidelobe levels in the off-axis antenna are better than those in the on-axis antenna, because in the on-axis design there will be diffraction, reflection, and blockage from the secondary mirror and its supports. An off-axis Gregorian telescope with correctly chosen offset angles will always be optically superior to a similar on-axis configuration. An offset telescope allows for large prime-focus instrument packages of the type used successfully on Python and other CMBR telescopes; these instruments *cannot* be used with an on-axis design.

In the proposed telescope, all optical elements are offset. The primary mirror consists of passively-mounted aluminum panels on a carbon-fiber reinforced polymer truss. The SP 10m will not use active surface technology where the panels of the primary are repositioned automatically; the primary is a passive structure which is manually adjusted. The secondary support, consisting of a large enclosed beam, permits the mounting of both a concave secondary mirror directed toward the Gregorian or Nasmyth foci and a prime focus instrumentation package for CMBR studies. A tertiary chopper is located at the exit pupil of the instrument, in a design similar to that used successfully on the AST/RO telescope.¹ The tertiary chopper can be repositioned to direct the beam to prime-focus packages, or removed to minimize the number of reflecting surfaces to the Gregorian focus. All mechanical systems are enclosed to protect them from the elements. Waste heat from compressors and motors will be ducted inside this enclosure. Both axes are fully balanced with counterweights.

Homology of the Primary Mirror— An important aspect of this antenna design is use of homology, that is, the tendency for gravity-induced primary mirror surface deflections to act as a focus shift. Simply stated, gravitational deflections must be parabolic and predictable, permitting their effect to be removed by a pre-calculated repositioning of the secondary mirror. Homologous primary mirror design is a particularly effective technique for a South Pole telescope, because gravitation rather than wind or temperature change is the dominant cause of structural deflections in the weather conditions prevalent at Pole.^{3,6} A structural analysis has been made of the preliminary primary mirror design which includes the panels, back-up structure, steel support, secondary, and mounting arrangement. For the preliminary analysis, a single-sized structural component was used throughout the reflector support truss. The analysis shows that the deflection in the primary resulting from a pointing change from zenith to an elevation angle of 50° follows a parabola to within 26 μm , or 16 μm RMS, with an absolute maximum deflection of 860 μm . This is surprisingly good, considering that the preliminary design has equal-stiffness truss elements and has not yet been optimized in any way. It therefore appears likely that the 10 meter primary can be designed to be diffraction-limited at 200 μm wavelength. The next step in the design is to iteratively modify the stiffness of the carbon-fiber truss rods, in order to improve the homology.

In further design studies we will consider various primary mirror support arrangements, examining the effects of the placement of the elevation axis and the ball screw elevation drive. We will perform a detailed analysis of the truss structure elements, optimizing the primary structural response, further reducing the primary mirror deflections,

Table 2. 10m Telescope Design Parameters.

optical performance		diffraction limited at 200 μm wavelength
field of view		at least 20' diameter
tracking		1" maximum error in winds of 10 m s^{-1} or less
slew speed		0.5 rpm in winds of 30 m s^{-1} or less
primary mirror homology		< 12 μm RMS deviation from defined surface
primary aperture	d	10000 mm
center of primary	I_2	(5300mm, 0, 1003.214mm)
paraxial focus of primary	F_1	(0, 0, 7000mm)
primary mirror materials		cast aluminum panels supported by carbon-fiber-reinforced-polymer truss and titanium nodes
panel size		each approximately 0.75 square meters
length along central ray from primary to secondary		8403.375 mm
center of secondary	I_1	(-265mm, 0, 7299.839mm)
first focus of secondary		(0, 0, 7000 mm)
second focus of secondary	F_0	(-11.16738mm, 0, -699.348mm)
diameter of secondary		700 mm
magnification of secondary	m	-20
scaleless backfocal distance	β	0.1
secondary materials		cast aluminum single panel
secondary mirror mount		actively-controlled hexapod
center of tertiary		(-251.616mm, 0, 6878.052mm)
chopping tertiary		opposed-torque balanced chopper
elevation drive system		counterweighted axis with ball screw drive or bull gear
azimuth drive system		opposed torque pinions on bull gear
azimuth bearing		fully-constrained gothic-arch with integral gear
encoder precision		23 bits
drive system electronics		VME/VXI bus system
detector focal points		prime focus (for CMBR), Gregorian, Nasmyth
Nasmyth cabin size		4 m \times 4 m \times 3 m
guide telescope		CCD camera at focus of 75 mm diameter f/9 lens

while improving the homology. A dynamical analysis of the primary mirror will consider the excitation of deflection modes by wind and by the drive system.

5. OPTICAL DESIGN

The optical design criteria are:

1. The field of view is diffraction-limited for wavelengths as short as $\lambda = 200\mu\text{m}$.
2. The illumination of the primary does not change significantly with chopper angle.
3. Large (1000 beam) focal plane arrays can be used in a protected environment.
4. The field of view is large enough to accommodate these large focal-plane arrays while beam chopping.

These requirements differ from those of visual-wavelength telescopes, where minimization of blockage and coma typically lead to a Ritchey-Chretien design, and also from those of most radio telescopes, where maximization of beam and aperture efficiency for the central beam typically leads to a classical Cassegrain configuration. The SP 10m is novel because a large field of view is needed in a situation where diffraction dominates the classical aberrations; in this case maximizing the flatness of the focal plane while providing a real exit pupil for the chopper location leads to a modified offset Gregorian design. The optics are offset in order to eliminate blockage, and the primary is shaped to enhance the field flatness.

The primary and secondary mirrors are symmetric about a vertical plane, and Figure 2 shows the intersection of this plane with the mirrors. This optical design has two more degrees of freedom than an on-axis telescope: the offset angles of the primary (i_2) and secondary (i_1) mirrors. Dragone²⁴ has shown that for an offset two mirror system the aberration function is equivalent to that of a single-mirror prime-focus paraboloid with offset angle i_0 , where

$$\tan i_0 = (1 - M)\tan i_1 + M \tan i_2, \quad (1)$$

where $M \equiv \frac{(F_0 I_1)}{(F_1 I_1)}$ is the off-axis magnification of the secondary. Aberrations are minimized if $\tan i_0 = 0$. Substituting this value into Equation 1 couples the two offset angles and reduces the number of degrees of freedom by one. An unfortunate effect of this relation is that the optical elements are then no longer rotationally symmetric about the z axis, greatly complicating the analysis of system properties. The final design of the optical system will be accomplished through numerical techniques, so this is not a fatal problem, but a simple analytic understanding of the effect of the design constraints and parameters is needed in the early stages of the design. If $|M|$ is large, a simplifying assumption can be made. The value of i_1 can be chosen so that the instrument focus lies on the z axis (i.e., at F_0 rather than F_{0D} in Figure 2). The system is then equivalent to an on-axis optical telescope with an off-axis aperture stop, and since that stop is large and admits at least some rays from all radial zones, the aberrations of the off-axis system are essentially the same as in the on-axis system. The value of i_0 is still sufficiently small that the aberrations of the resulting rotationally symmetric system are not very much greater than for the fully optimized system. An analytic solution can therefore be obtained for a system whose aberrations are only somewhat worse than those of the fully optimized design.

Consider a Gregorian design, and parameterize the mirror surfaces to allow deviations from the classical design in order to optimize the optical performance. An important practical constraint on this parameterization is that the primary be a section of a figure of revolution, so that the mirror panels in every row are identical. The discussion below follows Schroeder²⁵ in sign conventions and variable names. In the classical case, the secondary is a section of a prolate spheroid with foci at F_0 and F_1 , and the primary is paraboloidal with a focus at F_1 in Figure 2. The central ray is shown as a short dashed line. In this figure the telescope is looking toward the zenith, along the z axis. The coordinate system, (x, y, z) has its origin at the vertex of the primary mirror paraboloid, and the focus of the paraboloid is at $(0, 0, 7000 \text{ mm})$, so the surface of the primary mirror satisfies the equation

$$0 = x^2 + y^2 - 2R_1 z + (1 + K_1)z^2, \quad (2)$$

where $R_1 = 2f_1 = 14000 \text{ mm}$ is the radius of curvature at the vertex $(0, 0, 0)$, f_1 is the on-axis focal length, and K_1 is the conic constant of the primary. $K_1 = -1$ for a parabolic primary; this is the parameter which will be varied. The primary mirror is a piece of this surface bounded by a cylinder 10000mm in diameter, with its axis parallel to z at $x = 5300 \text{ mm}, y = 0$. The central ray follows this axis from $z = \infty$ until it intercepts the center of the primary mirror at $(5300 \text{ mm}, 0, 1003.2 \text{ mm})$, where it reflects at an angle of incidence $i_2 \approx 25^\circ$, through F_1 at $(0, 0, 7000 \text{ mm})$, to the center of the secondary. The equation of the secondary can be written:

$$0 = x^2 + y^2 - 2R_2(z - z_2) + (1 + K_2)(z - z_2)^2, \quad (3)$$

where R_2 is the on-axis radius of curvature (a negative number for a concave secondary), K_2 is the conic constant of the secondary, and z_2 is the distance between the vertex of the secondary and the vertex of the primary.

The condition that the paraxial rays have focal points at F_1 and F_0 gives

$$R_2 = \frac{m(1 + \beta)}{m^2 - 1} R_1 \quad (4)$$

and

$$z_2 = \frac{m - \beta}{2(m + 1)} R_1, \quad (5)$$

where m is the magnification of the secondary and β is the scaleless back focal length of the instrument, as shown in Figure 2. The effective focal length of the system is $f = mf_1$. Since the system is off-axis, the paraxial rays are not admitted by the aperture, but rays hitting the inner part of the mirror close to the z axis are nearly paraxial. Note that in a Gregorian system, m is negative. For definiteness, choose $m = -20$ and $\beta = 0.1$, parameters which result in a reasonably small secondary mirror and a useful distance between the secondary and the focus F_0 . Since m , β , and f_1 are fixed, R_1 , R_2 and z_2 are also fixed, while the conic constants of the mirrors, K_1 and K_2 , are varied.

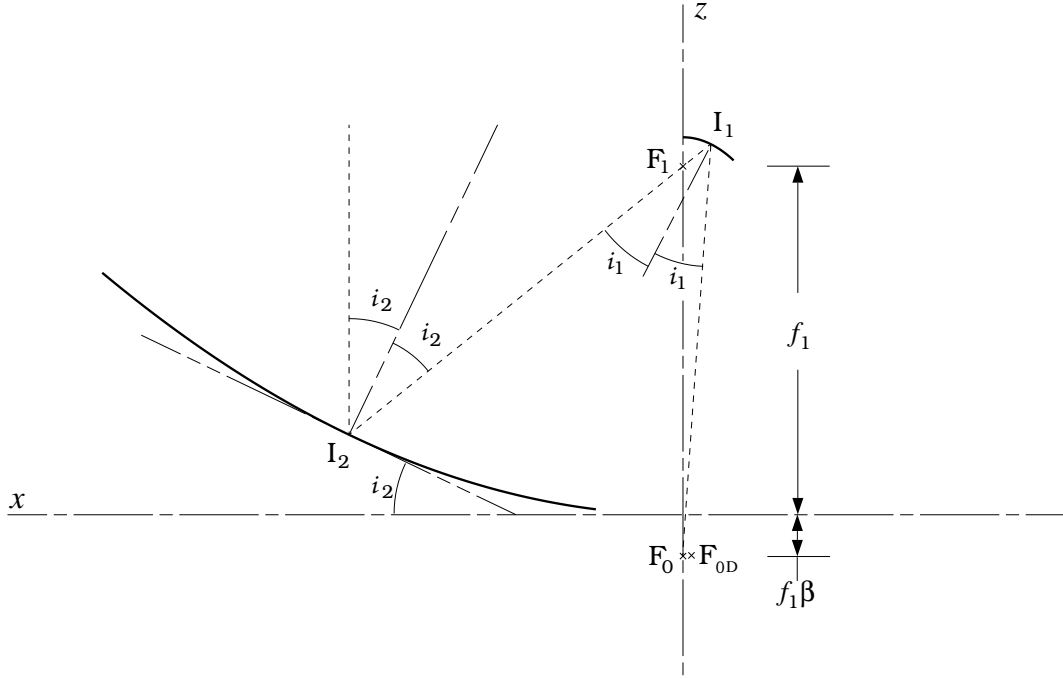


Figure 2. Scale drawing of the primary and secondary mirrors. The instrument focus indicated by F_{0D} satisfies the Dragone²⁴ relation, Equation 1 with $i_0 = 0$. The alternative focus indicated by F_0 nearly satisfies the Dragone relation while greatly simplifying the calculation of aberrations, since the line F_1F_0 is then the axis of symmetry of the mirrors, and the mirrors are figures of revolution: the telescope is then equivalent to an on-axis instrument with an off-axis aperture stop.

The condition that the focal point F_0 be free of spherical aberration gives a relation between the two conic constants:

$$K_2 = -\left(\frac{m+1}{m-1}\right)^2 + \frac{m^3(m+1)}{(1+\beta)(m-1)^3}(K_1+1) \equiv A + B(K_1+1). \quad (6)$$

In the case of a classical Gregorian, the additional requirement that the spherical aberration at F_1 be zero leads to a paraboloidal primary with $K_1 = -1$, so $K_2 = A = -0.819$ and the secondary is a prolate spheroid with focii at F_1 and F_0 . For the present design, there is no advantage to a sharp focus at F_1 , and no such requirement exists. The system therefore has one remaining degree of freedom, K_1 , which can be chosen to minimize aberrations and maximize image quality at F_0 .

Aberrations— The classical third-order optical aberrations for rays reflecting within the telescope can be written in terms of the parameters defined above.²⁵ Let x be the x -coordinate value of the point where a ray strikes the primary mirror, and θ be the angle on the sky between that ray and the central ray. The worst-case ray strikes the outer edge of the primary, where $x = 1030\text{mm}$. The angular tangential coma, θ_c , is

$$\theta_c = \frac{3\theta x^2}{4f^2} \left[1 + \frac{m^2(m-\beta)}{2(1+\beta)}(K_1+1) \right] \equiv \theta \frac{x^2}{f^2} [C + D(K_1+1)]. \quad (7)$$

The angular astigmatism, θ_a , is

$$\theta_a = -\frac{\theta^2 x}{f} \left[\frac{m^2 + \beta}{m(1+\beta)} - \frac{m(m-\beta)^2}{4(1+\beta)^2}(K_1+1) \right] \equiv \theta^2 \frac{x}{f} [E + F(K_1+1)]. \quad (8)$$

The curvature of the surface of best focus, κ_m , is

$$\kappa_m = \frac{1}{f} \left[\frac{(m^2 - 2)(m - \beta) + m(m + 1)}{m(1 + \beta)} - \frac{m(m - \beta)^2}{2(1 + \beta)^2} (K_1 + 1) \right] \equiv \frac{1}{f} [G + H(K_1 + 1)]. \quad (9)$$

Since the surface of best images cannot be too highly curved, the usable field of view on the sky cannot be much larger than

$$\theta_f = \frac{1}{f\kappa_m} = [G + H(K_1 + 1)]^{-1}, \quad (10)$$

the field angle at which the focal surface curvature is significant. The values of the coefficients A through H are listed in Table 3.

Table 3. Evaluation of Aberration Coefficients for $m = -20$, $\beta = 0.1$

A	B	C	D	E	F	G	H
-0.819	-14.92	0.75	-2877.	18.19	-1669.	346.4	3339.

In the evaluation of the aberrations for visual wavelength telescopes, it would at this point be noted that the dominant remaining aberration is coma, and the value of K_1 would be chosen so that $\theta_c = 0$ in Equation 7. This would result in a Ritchey-Chretien design for positive m and an aplanatic Gregorian design for negative m . In the aplanatic Gregorian case, K_1 would be slightly larger than -1 ($K_1 \approx -0.95$), resulting in an ellipsoidal primary. This eliminates third-order coma, but at the expense of a reduced field of view, θ_f .

For a submillimeter-wave telescope, however, the dominant source of blur at the focal surface is not coma but diffraction. The diffraction-limited resolution on the sky is $\theta_d = \lambda/d$, and $\theta_d > \theta_c$ for all field angles θ such that

$$\theta < \frac{\lambda f^2}{x^2 d} [C + D(K_1 + 1)]^{-1} \approx \frac{\lambda}{d} [C + D(K_1 + 1)]^{-1} F^2, \quad (11)$$

where $F \equiv f/d = mf_1/d$ is a large number. To put it another way, coma becomes significant compared to diffraction only for beams which are $\sim F^2/[D(K_1 + 1)]$ beam diameters away from the center, and $F^2 \sim 400$. (For visual wavelength telescopes this is a real limitation, since the diffraction-limited beamsize is $\lambda/d \sim 2 \times 10^{-7} = 0.04''$, and unless it is corrected, coma becomes significant $\sim 10''$ from the center of the field.)

Since diffraction swamps the classical aberrations, the size of the field of view in the submillimeter will tend to be dominated by curvature of the focal surface. Consider, for example, the classical Gregorian case $K_1 = -1$ in Equation 10: $\theta_f = G^{-1} = 0.0029 = 10'$. The size of the usable field of view can be enlarged by setting K_1 so as to maximize θ_f in Equation 10:

$$K_1 = -\frac{G}{H} - 1 = -1.10, \quad (12)$$

resulting in a hyperboloidal primary mirror. Substitution of this value into Equation 2 shows that the $K_1 = -1.1$ primary deviates from a paraboloid by $\Delta z = -50$ mm at the outer edge of the primary surface (10300 mm, 0, 3739 mm). Substitution into Equation 6 yields $K_2 = 0.67$, and Equation 3 shows that the secondary is then an oblate spheroid. Substitution in Equation 8 shows that this choice worsens the astigmatism, but not to a degree which is significant compared to diffraction. Substitution in Equation 11, however, shows that this choice of primary results in coma which is becoming important compared to diffraction. In the fully corrected system, where i_1 is chosen so that $i_0 = 0$ in Equation 1, the coma will be reduced by a factor of ~ 4 , so Equation 11 should be considered an upper bound to the significance of coma. There is, therefore, an optimal value for K_1 such that $-1.1 < K_1 < -1.0$ and the image is maximally flat and minimally aberrated.

An intriguing possibility sets $K_2 = 0$. Then the secondary is a concave sphere, and the exit pupil of the telescope, which in this design is the position of the tertiary chopper, lies near the center of that sphere. This choice provides some flattening of the focal surface (since $K_1 = -A/B - 1 = -1.055 < -1$), coma which is reduced compared to the $K_1 = -1.1$ case, and also a high degree of symmetry at the secondary mirror during the beam chop. This possibility will be investigated using numerical methods.

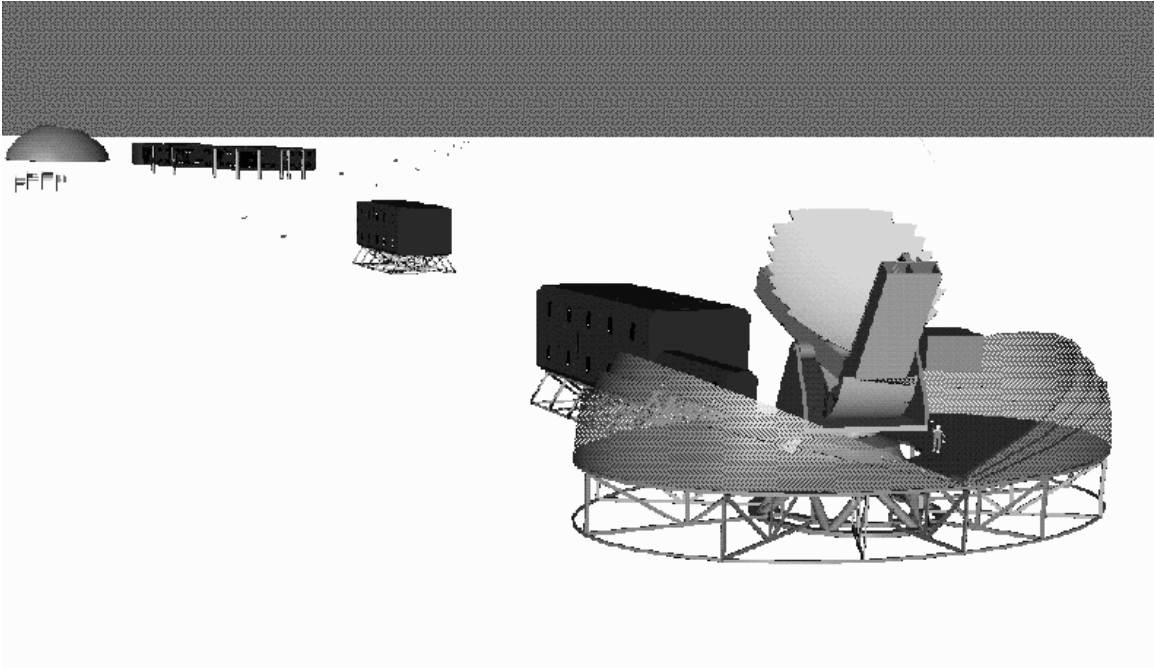


Figure 3. Computer model of the 10 meter telescope at South Pole. The new South Pole station, the existing dome and M. A. Pomerantz Laboratory are in the background. All surface buildings are elevated to reduce snow drifts. The 10 meter support facility will occupy one floor of the new Dark Sector laboratory building and connect to it by a covered walkway. A clamshell-shaped protective enclosure is shown in the stowed position.

6. CONSTRUCTION AND MANAGEMENT PLANS

The telescope will be constructed at the Smithsonian Submillimeter Array construction and test facility at Haystack Observatory during calendar year 2002. From 1999 through 2001, project personnel will fully specify the instrument, carry out trade studies and design and performance analysis. In the year 2003, the telescope will be tested using SMA test facilities. The telescope will be disassembled, packed, and then unpacked and re-assembled at Haystack Observatory. This will assure that the third assembly at the Pole proceeds as smoothly as possible. The telescope and all associated equipment will be repacked and delivered to the NSF Antarctic contractor in Port Hueneme, California. In 2004 and 2005, the telescope will be reassembled and commissioned at Pole.

The 10 meter telescope will be operated as a user-facility instrument by an international consortium. Observing time will be allocated with consideration for the contributions of the international partners, but will otherwise be freely available on a proposal basis. The strong survey capabilities of this instrument in the submillimeter and for CMBR argue that a large fraction of the time (70%) should be allocated in large blocks to several key projects. These key project blocks will be allocated at three year intervals in an open selection process involving a review of solicited proposals. Successful competitors for these key project blocks would likely design and construct detector packages. The remaining fraction of the observing time (30%) will be allocated to relatively smaller and less complex projects which use the existing detector packages. These projects will be carried out by remote observing techniques, in collaboration with SP 10m scientific staff.

ACKNOWLEDGMENTS

We thank P. Cheimets, D. Caldwell, W. Davis, and W. Bruckman for their work on the telescope design. We thank R. W. Wilson and A. P. Lane for their contributions to the 10 meter proposal. We are grateful to B. Elmegreen, D. Fischer, P. Goldsmith, A. Lane, and G. Knapp for their contributions to the science goals for the SP 10m.

This work was supported in part by the Smithsonian Institution and in part by the National Science Foundation under a cooperative agreement with the Center for Astrophysical Research in Antarctica (CARA), grant number NSF DPP 89-20223. CARA is a National Science Foundation Science and Technology Center.

REFERENCES

1. A. A. Stark, R. A. Chamberlin, J. Cheng, J. Ingalls, and G. Wright, "Optical and mechanical design of the Antarctic Submillimeter Telescope and Remote Observatory," *Rev. Sci. Instr.* **68**, p. 2200, 1997.
2. A. P. Lane, "Submillimeter transmission at the South Pole," in *Astrophysics from Antarctica*, G. Novak and R. H. Landsberg, eds., ASP Conferences Series, 1998.
3. W. Schwerdtfeger, *Weather and Climate of the Antarctic*, Elsevier, 1984.
4. R. A. Chamberlin and J. Bally, "225 GHz atmospheric opacity of the South Pole sky derived from continual radiometric measurements of the sky-brightness temperature," *Appl. Opt.* **33**(6), p. 1095, 1994.
5. R. A. Chamberlin and J. Bally, "The observed relationship between the South Pole 225-GHz atmospheric opacity and the water vapor column density," *Int. J. Infrared Millimeter Waves* **16**(5), p. 907, 1995.
6. R. A. Chamberlin, A. P. Lane, and A. A. Stark, "The 492 GHz atmospheric opacity at the geographic south pole," *ApJ* **476**, p. 428, 1997.
7. Y. Rephaeli, "Comptonization of the cosmic microwave background: The Sunyaev-Zel'dovich effect," *Ann. Rev. Astron. & Astrophys.* **33**, p. 541, 1995.
8. G. R. Meurer, "The case for substantial dust extinction at $z \approx 3$," 1998. astro-ph/9708163.
9. C. Pearson and M. Rowan-Robinson, "Starburst galaxy contributions to extragalactic source counts," *MNRAS* **283**, p. 174, 1996.
10. I. Smail, R. J. Ivison, and A. W. Blain, "A deep sub-millimeter survey of lensing clusters: A new window on galaxy formation and evolution," *ApJ*, 1998. astro-ph/9708135.
11. A. R. Sandage, R. G. Kron, and M. S. Longair, *The Deep Universe*, vol. 23 of *Saas-Fee Advanced Course*, ch. Longair 11, pp. 500–514. Springer, 1995.
12. A. W. Blain, "Galaxy-galaxy gravitational lensing in the millimetre/submillimetre waveband," *MNRAS* **383**, p. 1340, 1996.
13. A. W. Blain and M. S. Longair, "Observing strategies for blank-field surveys in the submillimetre waveband," *MNRAS* **278**, p. 847, 1996.
14. D. Hughes and J. Dunlop, "Using new submillimetre surveys to identify the evolutionary status of high- z galaxies," in *Observational Cosmology with New Radio Surveys*, 1997. Preprint available on WWW at <http://www.roe.ac.uk/research/dhh2.ps.gz>.
15. D. H. Hughes, J. S. Dunlop, and S. Rawlings, "High-redshift radio galaxies and quasars at sub-millimetre wavelengths: assessing their evolutionary status," *MNRAS* **289**, p. 766, 1997.
16. G. J. Stacey, N. Geis, R. Genzel, J. B. Lugten, A. Poglitsch, A. Sternber, and C. H. Townes, "The 158 micron [C II] line: a measure of global star formation activity in galaxies," *ApJ* **373**, p. 423, 1991.
17. E. L. Wright, J. C. Mather, C. L. Bennett, E. S. Cheng, R. A. Shafer, D. J. Fixsen, R. E. Eplee, Jr., R. B. Isaacman, S. M. Read, N. W. Boggess, S. Gulkis, M. G. Hauser, M. Janssen, T. Kelsall, P. M. Lubin, S. S. Meyer, S. H. Moseley, T. L. Murdock, R. F. Silverberg, G. F. Smoot, R. Weiss, and D. T. Wilkinson, "Preliminary spectral observations of the galaxy with a 7° beam by the COsmic Background Explorer (COBE)," *ApJ* **381**, p. 200, 1991.
18. V. Petrosian, J. Bahcall, and E. E. Salpeter, "Fine structure transitions and the microwave background," *ApJ (Letters)* **155**, p. L57, 1969.
19. A. Loeb, "Finding protoquasars at high redshifts," *ApJ (Letters)* **404**, p. 37, 1993.
20. A. A. Stark, "Potential measurement of the luminosity function of 158 micron [C II] at high redshifts: a test of galaxy formation models," *ApJ* **481**, p. 587, 1997.
21. R. H. Hildebrand, J. Dotson, C. D. Dowell, S. R. Platt, D. Schleuning, J. A. Davidson, and G. Novak, "Far-infrared polarimetry," in *Airborne Astronomy Symposium on the Galactic Ecosystem*, M. R. Haas, J. A. Davidson, and E. F. Erickson, eds., vol. 73, p. 97, ASP Conf. Ser., 1995.
22. F. H. Shu, S. Lizano, and F. C. Adams, "Star formation in molecular cloud cores," in *Star Forming Regions, IAU Symp. 115*, M. Peimbert and J. Jugaku, eds., p. 417, Kluwer, 1987.

23. A. A. Stark, A. D. Bolatto, R. A. Chamberlin, A. P. Lane, T. M. Bania, J. M. Jackson, and K.-Y. Lo, "First detection of 492 GHz [C I] emission from the Large Magellanic Cloud," *ApJ (Letters)* **480**, p. L59, 1997.
24. C. Dragone, "A first-order treatment of aberrations in cassegrainian and gregorian antennas," *IEEE Trans. Antennas and Propagation* **AP-30**, p. 331, 1982.
25. D. J. Schroeder, *Astronomical Optics*, Academic Press, 1987.